Received: 23 January 2018 | Revised: 13 March 2018 | Accepted: 20 March 2018

DOI: 10.1002/aoc.4392

Check for updates

FULL PAPER

WILEY Applied Organometallic Chemistry

Metal complexes of novel Schiff base derived from the condensation of 2-quinoline carboxaldehyde and ambroxol drug with some transition metal ions

Walaa H. Mahmoud[1] | Gehad G. Mohamed[1,2] | Hoda A. Elsawy[3] | Mostafa A. Radwan[3]

[1] Chemistry Department, Faculty of Science, Cairo University, Giza 12613, Egypt

[2] Egypt Nanotechnology Center, 6th October City, El-Sheikh Zayed, Giza, Egypt

[3] Chemical Engineering Department, Faculty of Engineering, British University in Egypt, Cairo, Egypt

Correspondence
Gehad G. Mohamed, Chemistry Department, Faculty of Science, Cairo University, Giza, 12613, Egypt.
Email: ggenidymohamed@sci.cu.edu.eg

A new Schiff base was prepared as the condensation product of the reaction of 2-quinoline carboxaldehyde and ambroxol drug. The Schiff base ligand thus obtained (HL; *trans*-4-[(2-(2-quinolinoimino)-3,5-dibromobenzyl)amino] cyclohexanol) was further employed as a tridentate ligand for the synthesis of new complexes through reaction with Cr(III), Mn(II), Fe(III), Co(II), Ni(II), Cu(II), Zn(II) and Cd(II) metal ions. The synthesized HL and its metal complexes were characterized using various physicochemical techniques including elemental analysis, Fourier transform infrared and UV–visible spectroscopies, conductimetric and magnetic susceptibility measurements, mass spectrometry and thermal analyses. ^{1}H NMR data indicated that complex formation was through the amino group rather than the aliphatic hydroxyl group. Thermal analysis gave an idea about the decomposition pattern of HL and its complexes. Also, it revealed the number of water molecules in the inner and outer spheres of the complexes. An octahedral geometry for all the complexes has been suggested. HL and its complexes were screened for their antimicrobial activity against various species of bacteria and fungi using the disc diffusion method. The Cr(III) complex had the highest antimicrobial activity.

KEYWORDS
ambroxol, antimicrobial activity, physicochemical techniques, Schiff base, TG/DTG

1 | INTRODUCTION

Schiff base ligands have a very crucial role in the field of coordination compounds. They can be found in the form of bidentate or tridentate ligands that are well known to coordinate with most transition metal ions, and their complexes are well reported. Reactions of Schiff bases are considered an important pathway in designing carbon–nitrogen bonds. Schiff bases and their metal complexes have found vast applications in many fields like industrial, agricultural and pharmaceutical chemistry.[1] They also have the ability to act as catalysts as well as anticorrosion agents.[2] Schiff bases also have very important features including high synthetic flexibility, high selectivity to the central metal atom and structural similarity to naturally occurring biological systems. The presence of the azomethine group (—N═CH—) has enabled the elucidation of the mechanism of racemization as well as transformation reaction within several biological systems.[3] Therefore, there is a need for further studies and reports of such Schiff base complexes. Schiff base ligands as well as their complexes with transition metals have recently acquired a well-deserved and a crucial importance that is attributed to their range of spectroscopic characteristics as well as their notable antibacterial, antifungal and antitumour activities.[4]

 Copyright © 2018 John Wiley & Sons, Ltd.

Pyridine, one of the most common heterocyclic reagents, has found application in many therapeutic compounds.[5] Consequently, pyridine-based Schiff base ligands can be promising in the fields of metal coordination, host–guest systems, extraction, enzyme mimics, antibiotics and natural products such as marine alkaloids.[6]

Ambroxol is a secretolytic agent that is mainly employed for the purpose of therapeutic treatment of some respiratory bronchopulmonary syndromes associated with excessive and abnormal mucus secretion, and impaired mucus transport. It is well known to enhance mucus clearance, to aid expectoration and to stimulate positive coughing, which would enable patients to breathe properly.[7] Ambroxol is a potent inhibitor of the neuronal Na^+ channels.[8] Ambroxol helps in easing pain in acute sore throat, a syndrome that is known as a side effect of acute pharyngitis.[9] Ambroxol has been reported to enhance the activity of the lysosomal enzyme glucocerebrosidase. Consequently further research is being conducted on its possible use as a treatment for both Gaucher disease and Parkinson's disease.[10] The ambroxol drug, suggested within this study, contains a primary amine group (NH_2) which can further react with an aldehyde or ketone to form a Schiff base compound.

In the study presented here, a novel Schiff base ligand was synthesized by the condensation of 2-quinoline carboxaldehyde with ambroxol drug. Its mode of chelation with various transition metal ions was examined, as well as the antimicrobial activity of the resulting chelates. Several spectroscopic techniques were employed for carrying out characterization of the prepared metal complexes.

2 | EXPERIMENTAL

2.1 | Materials and Reagents

All chemicals used were of analytical reagent grade, and of the highest purity available. They included 2-quinoline carboxaldehyde, ambroxol, $CrCl_3{\cdot}6H_2O$, $MnCl_2{\cdot}2H_2O$, $FeCl_3{\cdot}6H_2O$, $CoCl_2{\cdot}6H_2O$, $NiCl_2{\cdot}6H_2O$, $CuCl_2{\cdot}2H_2O$, $ZnCl_2$ and $CdCl_2$, which were obtained from Aldrich, Nile Pharma, Sigma, Sigma, Prolabo, Sigma, BDH, Aldrich and Aldrich, respectively. Chemicals used for the anticancer study included dimethylsulfoxide (DMSO), RPMI-1640 medium, sodium bicarbonate, isotonic trypan blue, penicillin, streptomycin, acetic acid, trypsin, trichloroacetic acid and sulforhodamine-B, provided by Sigma Chemical Co., St Louis, MO, USA. Organic solvent used was ethyl alcohol (99 and 95%). Deionized water was usually used in all preparations.

2.2 | Solutions

Fresh stock solution of the Schiff base ligand (1×10^{-3} M) was prepared by dissolving an accurately weighed amount (0.4 g l^{-1}) in the appropriate volume of ethyl alcohol. Solutions of the ligand and its metal complexes (1×10^{-4} and 1×10^{-5} M) were prepared by appropriate dilution of the previously prepared stock solutions for measuring their UV–visible spectra.

2.3 | Instrumentation

Mass spectra were recorded using the EI technique at 70 eV with an MS-5988 GS-MS Hewlett-Packard instrument at the Microanalytical Center, National Center for Research, Egypt. Molar conductivities of 10^{-3} M solutions of the complexes in ethanol were measured using a Jenway 4010 conductivity meter. Molar magnetic susceptibility was measured on powdered samples using the Faraday method. The diamagnetic corrections were made using Pascal's constant and $Hg[Co(SCN)_4]$ was used as a calibrant. Microanalyses of carbon, hydrogen and nitrogen were carried out at the Microanalytical Center, Cairo University, Egypt, using a CHNS-932 (LECO) Vario elemental analyser. Analyses of the metals followed the dissolution of the solid complexes in concentrated HNO_3, neutralizing the diluted aqueous solutions with ammonia and titrating the metal solutions with EDTA. Fourier transform infrared (FT-IR) spectra were recorded with a PerkinElmer 1650 spectrometer (400–4000 cm^{-1}) in KBr pellets. Electronic spectra were recorded at room temperature with a Shimadzu 3101pc spectrophotometer as solutions in ethanol. ^1H NMR spectra, with samples as solutions in DMSO-d_6, were recorded with a 300 MHz Varian-Oxford Mercury at room temperature using tetramethylsilane (TMS) as an internal standard. UV–visible spectra were obtained with a UV mini-1240 spectrophotometer (Shimadzu). Thermogravimetric (TG) and differential thermogravimetric (DTG) analyses of the solid complexes were carried out from room temperature to 1000 °C using a Shimadzu TG-50H thermal analyser. Optical density was measured spectrophotometrically at 564 nm with an ELIZA microplate reader (R 960, Meter Tech, USA). The antimicrobial activities were determined at the Microanalytical Center, Cairo University, Egypt.

2.4 | Synthesis of Schiff Base Ligand

The Schiff base ligand *trans*-4-[(2-(2-quinolinoimino)-3,5-dibromobenzyl)amino]cyclohexanol (HL) was prepared by refluxing a mixture of 2-quinoline carboxaldehyde (6.61 mmol, 1.04 g) with ambroxol (6.61 mmol, 2.5 g)

dissolved in ethanol. The resulting mixture was stirred under reflux for about 2 h at 100–150 °C during which a reddish brown solid compound was separated. It was filtered, recrystallized, washed with dimethylformamide (DMF) and dried in vacuum (Scheme 1).

Yield 92%; m.p. 140 °C; reddish brown solid. Anal. Calcd for $C_{23}H_{23}Br_2N_3O$ (%): C, 53.38; H, 4.45; N, 8.12. Found (%): C, 53.21; H, 4.24; N, 8.02. FT-IR (cm^{-1}): hydroxyl ν(OH) 3422, azomethine ν(C═N) 1630, pyridine ring stretching 1074, amino ν(NH) bending 618. ^1H NMR (300 MHz, DMSO-d_6, δ, ppm): 7.50–8.65 (m, 8H, Ar H), 9.21 (s, 1H, azomethine), 4.90 (s, 1H, aliphatic OH), 4.06 (s, 1H, NH). UV–visible (λ_{max}, nm): 230 (π–π*), 302 (n–π*).

2.5 | Synthesis of Metal Chelates

The metal complexes were prepared by the addition of a hot solution (60 °C) of the appropriate metal chloride (0.77 mmol) in ethanol (25 ml) to a hot solution (60 °C) of HL (0.4 g l^{-1}, 0.77 mmol) in ethanol (25 ml). The resulting mixture was stirred under reflux for 2 h whereupon the complexes precipitated. They were removed by filtration, washed with a small amount of hot DMF and dried in vacuum desiccators over anhydrous calcium chloride. The analytical data for C, H and N were obtained in duplicate.

[Cr(HL)(H$_2$O)Cl$_2$]Cl·4H$_2$O.

Yield 87%; grey solid, m.p. 148 °C. Anal. Calcd for $C_{23}H_{33}Cl_3CrBr_2N_3O_6$ (%): C, 36.05; H, 4.31; N, 5.49; Cl, 13.91; Cr, 6.79. Found (%): C, 36.02; H, 4.12; N, 5.10; Cl, 13.37; Cr, 6.34. FT-IR (cm^{-1}): hydroxyl ν(OH) 3414, azomethine ν(C═N) 1627, pyridine ring stretching 1065, amino ν(NH) bending 610, ν(H$_2$O) stretching of coordinated water 870 and 756, ν(M—O) of coordinated water stretching 510, ν(M—N) stretching 472. UV–visible (λ_{max}, nm): 238 (π–π*), 304 (n–π*). Diffuse reflectance spectra (ν, cm^{-1}): 24 639, 20 465 and 14 813, attributed to $^4A_{2g}(F) \rightarrow {}^4T_{2g}(F)$, $^4A_{2g}(F) \rightarrow {}^4T_{1g}(F)$ and $^4A_{2g}(F) \rightarrow {}^4T_{2g}(P)$ transitions, respectively.

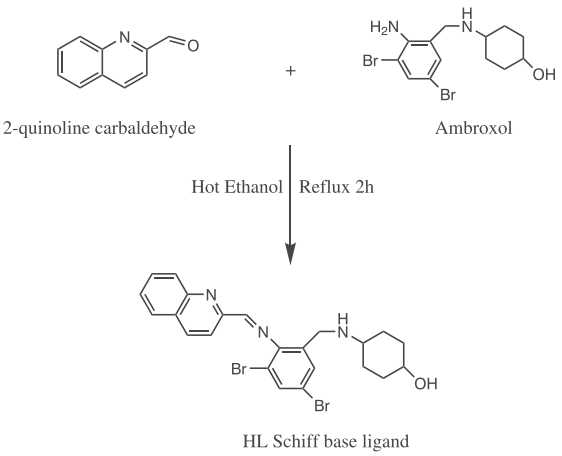

SCHEME 1 Synthesis of Schiff base ligand HL

[Mn(HL)(H$_2$O)$_2$Cl]Cl·3H$_2$O

Yield 82%; dark brown solid, m.p. 152 °C. Anal. Calcd for $C_{23}H_{33}Cl_2MnBr_2N_3O_6$ (%): C, 37.65; H, 4.50; N, 5.73; Cl, 9.69; Mn, 7.50. Found (%): C, 37.45; H, 4.23; N, 5.61; Cl, 9.56; Mn, 7.22. FT-IR (cm^{-1}): hydroxyl ν(OH) 3414, azomethine ν(C═N) 1625, pyridine ring stretching 1065, amino ν(NH) bending 613, ν(H$_2$O) stretching of coordinated water 867 and 767, ν(M—O) of coordinated water stretching 543, ν(M—N) stretching 481. UV–visible (λ_{max}, nm): 244 (π–π*), 302 (n–π*). Diffuse reflectance spectra (ν, cm^{-1}): 14 763, 20 355, 24 614 and 30 230, assigned to $^6A_{1g} \rightarrow {}^4T_{1g}(4G)$, $^6A_{1g} \rightarrow {}^4E_g$, $^6A_{1g} \rightarrow {}^4E_g(4D)$ and $^6A_{1g} \rightarrow {}^4T_{1g}(4P)$ transitions, respectively.

[Fe(HL)Cl$_3$]·5.5H$_2$O

Yield 79%; dark brown solid, m.p. 160 °C. Anal. Calcd for $C_{23}H_{31}Cl_3FeBr_2N_3O_{6.5}$ (%): C, 35.60; H, 4.01; N, 5.42; Cl, 13.74; Fe, 7.20. Found (%): C, 35.32; H, 3.79; N, 5.26; Cl, 13.51; Fe, 7.04. FT-IR (cm^{-1}): hydroxyl ν(OH) 3397, azomethine ν(C═N) 1629, pyridine ring stretching 1069, amino ν(NH) bending 620, ν(M—N) stretching 445. UV–visible (λ_{max}, nm): 243 (π–π*), 303 (n–π*). Diffuse reflectance spectra (ν, cm^{-1}): 35 462, 26 672 and 22 805, assigned to $^6A_{1g} \rightarrow {}^6T_{2g}(G)$ and $^6A_{1g} \rightarrow {}^6T_{1g}$ transitions, respectively, and 47 850 (ligand-to-metal charge transfer).

[Co(HL)(H$_2$O)$_2$Cl]Cl

Yield 75%; dark brown solid, m.p. 143 °C. Anal. Calcd for $C_{23}H_{27}Cl_2CoBr_2N_3O_3$ (%): C, 40.41; H, 3.95; N, 6.15; Cl, 10.40; Co, 8.64. Found (%): C, 40.33; H, 3.88; N, 6.00; Cl, 10.29; Co, 8.45. FT-IR (cm^{-1}): hydroxyl ν(OH) 3401, azomethine ν(C═N) 1625, pyridine ring stretching 1064, amino ν(NH) bending 614, ν(H$_2$O) stretching of coordinated water 868 and 767, ν(M—O) of coordinated water stretching 551, ν(M—N) stretching 453. UV–visible (λ_{max}, nm): 238 (π–π*), 302 (n–π*). Diffuse reflectance spectra (ν, cm^{-1}): 16 436, 17 382 and 21 102, assigned to $^4T_{1g}(F) \rightarrow {}^4T_{2g}(F)$, $^4T_{1g}(F) \rightarrow {}^4A_{2g}(F)$ and $^4T_{1g}(F) \rightarrow {}^4T_{1g}(P)$ transitions, respectively.

[Ni(HL)(H$_2$O)$_2$Cl]Cl

Yield 80%; dark brown solid, m.p. 156 °C. Anal. Calcd for $C_{23}H_{27}Cl_2NiBr_2N_3O_3$ (%): C, 40.43; H, 3.95; N, 6.15; Cl, 10.40; Ni, 8.60. Found (%): C, 40.30; H, 3.83; N, 6.02; Cl, 10.25; Ni, 8.49. FT-IR (cm^{-1}): hydroxyl ν(OH) 3395, azomethine ν(C═N) 1626, pyridine ring stretching 1066, amino ν(NH) bending 620, ν(H$_2$O) stretching of coordinated water 856 and 746, ν(M—O) of coordinated water

stretching 525, ν(M—N) stretching 465. UV–visible (λ_{max}, nm): 233 (π–π^*), 303 (n–π^*). Diffuse reflectance spectra (ν, cm^{-1}): 16 736, 18 215 and 25 801, assigned to: $^3A_{2g}(F) \rightarrow {}^3T_{2g}(F)$, $^3A_{2g}(F) \rightarrow {}^3T_{1g}(F)$ and $^3A_{2g}(F) \rightarrow {}^3T_{2g}(F)$ transitions, respectively.

$[Cu(HL)(H_2O)_3]Cl_2$

Yield 77%; dark brown solid, m.p. 158 °C. Anal. Calcd for $C_{23}H_{29}Cl_2CuBr_2N_3O_4$ (%): C, 39.12; H, 4.11; N, 5.95; Cl, 10.06; Cu, 9.00. Found (%): C, 38.94; H, 4.02; N, 5.81; Cl, 9.83; Cu, 8.87. FT-IR (cm^{-1}): hydroxyl ν(OH) 3417, azomethine ν(C═N) 1625, pyridine ring stretching 1064, amino ν(NH) bending 616, $\nu(H_2O)$ stretching of coordinated water 870 and 766, ν(M—O) of coordinated water stretching 534, ν(M—N) stretching 457. UV–visible (λ_{max}, nm): 244 (π–π^*), 302 (n–π^*). Diffuse reflectance spectra (ν, cm^{-1}): 16 413, 19 586 and 26 805, assigned to $^2B_{1g} \rightarrow {}^2A_{1g}(d_{x^2-y^2} \rightarrow d_{z^2})$, $^2B_{1g} \rightarrow {}^2B_{2g}(d_{x^2-y^2} \rightarrow d_{xy})$ and $^2B_{1g} \rightarrow {}^2E_g(d_{x^2-y^2} \rightarrow d_{xz}, d_{yz})$ transitions, respectively.

$[Zn(HL)(H_2O)_2Cl]Cl{\cdot}2H_2O$

Yield 82%; brown solid; m.p. 143 °C. Anal. Calcd for $C_{23}H_{32}Cl_2ZnBr_2N_3O_5$ (%): C, 38.01; H, 4.41; N, 5.79; Cl, 9.79; Zn, 9.02. Found (%): C, 37.86; H, 4.23; N, 5.56; Cl, 9.56; Zn, 8.82. FT-IR (cm^{-1}): hydroxyl ν(OH) 3434, azomethine ν(C═N) 1625, pyridine ring stretching 1064, amino ν(NH) bending 603, $\nu(H_2O)$ stretching of coordinated water 866 and 771, ν(M—O) of coordinated water stretching 515, ν(M—N) stretching 467. ^{1}H NMR (300 MHz, DMSO-d_6, δ, ppm): 7.42–8.22 (m, 8H, Ar H), 9.11 (s, 1H, azomethine), 4.91 (s, 1H, aliphatic OH), 4.11 (s, 1H, NH). UV–visible (λ_{max}, nm): 238 (π–π^*), 302 (n–π^*).

$[Cd(HL)(H_2O)Cl_2]{\cdot}2H_2O$

Yield 86%; brown solid; m.p. 165 °C. Anal. Calcd for $C_{23}H_{29}Cl_2CdBr_2N_3O_4$ (%): C, 36.60; H, 3.85; N, 5.57; Cl, 9.42; Cd, 14.85. Found (%): C, 36.35; H, 3.59; N, 5.36; Cl, 9.26; Cd, 14.56. FT-IR (cm^{-1}): hydroxyl ν(OH) 3425, azomethine ν(C═N) 1629, pyridine ring stretching 1072, amino ν(NH) bending 616, $\nu(H_2O)$ stretching of coordinated water 864 and 768, ν(M—O) of coordinated water stretching 530, ν(M—N) stretching 445. UV–visible (λ_{max}, nm): 241 (π–π^*), 303 (n–π^*).

2.6 | Antimicrobial Activity

Filter paper discs (5 mm) were transferred into 250 ml flasks containing 20 ml of working volume of test solutions (100 mg ml^{-1}). All flasks were autoclaved for 20 min at 121 °C. LB agar media surfaces were inoculated with four investigated bacteria (Gram-positive bacteria: *Bacillus subtilis* and *Staphylococcus aureus*; Gram-negative bacteria: *Salmonella* species and *Escherichia coli*) and fungi (*Aspergillus fumigates* and *Candida albicans*) using the diffusion agar technique,[11–13] then transferred to a saturated disc with a test solution in the centre of a Petri dish (agar plates). All compounds were placed at four equidistant positions at a distance of 2 cm from the centre in the inoculated Petriplates. DMSO served as control. Finally, all these Petri dishes were incubated at 25 °C for 48 h where clear or inhibition zones were detected around each disc. Control flask of the experiment was designed to perform under the same conditions described previously for each microorganism but with DMF solution only and by subtracting the diameter of inhibition zone resulting with DMF from that obtained in each case, so antimicrobial activity could be calculated.[14,15] Amikacin and ketokonazole were used as reference compounds for antibacterial and antifungal activities, respectively. All experiments were performed in triplicate and data plotted were the mean values.

2.7 | Molecular Docking

For the possibility of finding the most suitable binding modes of the most active compounds against RNA of amikacin antibiotic (PDB ID: 4P20) and human serum albumin (PDB ID: 5fuo), molecular docking studies were implemented via the usage of Autodock MOA2008 software. This is a molecular docking program[16] and is a cooperative molecular graphics software used in calculating and demonstrating realistic docking modes of a receptor, ligand and complex molecules. It requires the input of the ligand and the receptor to be in PDB format. The amino acid chain was preserved and the water molecules and co-crystallized ligands were detached. The ligand structure in PDB file format was generated using Gaussian09 software. The crystal structures of the RNA of amikacin antibiotic (PDB ID: 4P20) and human serum albumin (PDB ID: 5fuo) were taken from the protein statistics bank.[17]

3 | RESULTS AND DISCUSSION

3.1 | Characterization of Schiff Base Ligand

Reddish brown HL was prepared by the reaction of 2-quinoline carboxaldehyde with ambroxol drug in a 1:1 ratio.

The FT-IR spectrum of HL ligand showed a lack of the NH_2 stretching band characteristic of ambroxol and C═O band of 2-quinoline carboxaldehyde. On the other hand, a new, strong and sharp vibration band appeared

at 1630 cm^{-1} due to the azomethine group (C═N), indicating the formation of the Schiff base product (HL).[18]

The ^1H NMR spectrum was obtained to confirm the ligand structure and its purity. This was done in DMSO-d_6 solution using TMS as internal standard.[19] The singlet signal at 9.21 ppm may be attributed to the azomethine CH proton. The multiple in the region 7.50–8.65 ppm may be attributed to the aromatic ring protons. The singlet signal of the aliphatic OH group appeared at 4.90 ppm and the cyclohexane protons appeared as a multiplet in the region 3.32–3.47 ppm. Furthermore, the singlet signal of the NH group appeared at 4.09 ppm.

The mass spectrum of the ligand exhibited a molecular ion peak at m/z = 516.85 amu corresponding to $[M]^+$, which confirmed the proposed formula $[C_{23}H_{23}Br_2N_3O]^+$ with atomic mass of 517 amu.

The elemental analysis data obtained were in good agreement with those for the suggested calculated formula which indicated that the ligand had the molecular formula $C_{23}H_{23}Br_2N_3O$.

3.2 | Characterization of Metal Complexes

All the complexes were coloured and stable in air. They were soluble in many organic solvents including ethanol. The complexes were characterized using various techniques such as elemental, FT-IR spectral, ^1H NMR spectral, mass spectral and thermal analyses.

3.2.1 | Elemental analysis

Metal complexes of HL were synthesized by the reaction of ethanoic solutions of Schiff base and each metal salt in 1:1 ratio and they had the composition of MHL type. The experimental elemental analysis of the complexes was to a large degree in agreement with the theoretical calculations. The data of the elemental analyses of metal complexes (C, H, N, Cl and M) are presented in Section 2.

3.2.2 | FT-IR spectra and mode of bonding

The FT-IR spectra of the formed complexes were compared with that of the free ligand to distinguish the coordination sites of chelation. The details are mentioned in Section 2. The FT-IR spectrum of HL exhibited a band at 1630 cm^{-1} documented for the azomethine ν(C═N) group.[20,21] This band was shifted to lower frequency in the spectra of all the complexes in the range 1625–1629 cm^{-1},[22] indicating the involvement of azomethine nitrogen in the chelation to the metal ions.[23] It was hard to characterize the stretching band of ν(NH) due to its overlapping with the ν(OH) stretching band. The stretching band of the pyridine ring was observed in the spectrum of the free ligand at 1074 cm^{-1} which was shifted for all the complexes to appear at 1064–1072 cm^{-1} indicating the participation of the pyridine ring in the complexation process. The ν(NH) bending band was observed for the free ligand at 618 cm^{-1} which was shifted for all of the complexes to 603–622 cm^{-1} indicating the linkage between the metal ions and the nitrogen atom. New bands for all complexes appeared in the region 410–481 cm^{-1} attributed to ν(M—N).[24] The bands in the region 510–553 cm^{-1} in the spectra of all the complexes were assigned to ν(M—O) stretching vibration of coordinated water.[19] Also, two new $\nu(H_2O)$ bands of coordinated water molecules appeared in the FT-IR spectra of the metal complexes at 818–871 and 746–771 cm^{-1}, indicating the binding of water molecules to the metal ions.[25] Accordingly, the HL ligand acted as a neutral tridentate chelating agent, bonded to the metal ion via three nitrogen atoms of the Schiff base. The formation of octahedral complexes was obtained through coordination with water molecules and chloride ions in all complexes.

3.2.3 | ^1H NMR spectral studies of metal complexes

The ^1H NMR spectra of the free Schiff base ligand and its Zn(II) complex were obtained by dissolving them in DMSO-d_6 and using TMS as internal standard. The chemical shifts of the different types of protons in the ^1H NMR spectra of the ligand and its Zn(II) complex were recorded. The aromatic ring protons showed as multiplets in the ranges 7.50–8.65 and 7.42–8.22 ppm for HL and its Zn(II) complex, respectively. The singlet signal at 4.06 ppm in the spectrum of the Schiff base ligand, which may be attributed to NH group, was shifted to appear at 4.11 ppm in the spectrum of the Zn(II) complex indicating its participation in the chelation process. On the other hand, the singlet signal that appeared at 4.90 ppm for the free ligand can be assigned to aliphatic OH. This singlet band of aliphatic OH did not change in the spectra of metal complexes which proved that it did not have any cooperative role in metal complex formation. The multiplet signal of the cyclohexane protons appeared in the same region as for the free ligand (3.32–3.47 ppm). It was concluded from the previous data that HL acted as neutral ligand during the complexation process.[26]

3.2.4 | Mass spectral studies

The mass spectrum of the Fe(III) complex revealed a molecular ion peak at m/z 775.98 amu which was coincident with the calculated weight of 778.50 amu. This result confirmed the stoichiometry of this complex as being of

[MHL] type. On the other hand, the peak of the parent ligand in the mass spectrum of the Fe(III) complex appeared at m/z 514.99 amu.

3.2.5 | Molar conductance measurements

The molar conductance (Λ_m) can be estimated from the relation $\Lambda_m = K/C$, where C is the molar concentration of the metal complex solution. In the complexation process, HL acted as a neutral tridentate ligand. The molar conductance was measured by dissolving 10^{-3} M of the ligand in ethanol at 25 °C using the recommended procedure. The data are given in Section 2.

It was evident from the results that Fe(III) and Cd(II) complexes had molar conductance values of 41 and 46 Ω^{-1} mol^{-1} cm^2, respectively, indicating their weakly ionic nature (non-electrolytes). This confirmed that the anions were involved in the coordination sphere. [37] While the Cr(III), Mn(II), Co(II), Ni(II) and Zn(II) complexes had molar conductance values of 97, 87, 74, 93 and 66 Ω^{-1} mol^{-1} cm^2, respectively, indicating the ionic nature of these complexes and that they were of type 1:1 electrolytes. But in the case of the Cu(II) complex, the molar conductance value was found to be 113 Ω^{-1} mol^{-1} cm^2, indicating that this complex was a 1:2 electrolyte.

3.2.6 | Electronic spectra and magnetic moment measurements

Electronic spectra of HL and its complexes were recorded at room temperature. The spectrum of HL showed a band at 230 nm, assigned to $\pi \rightarrow \pi^*$ transition of the aromatic rings. In addition, strong bands also appeared at 302 nm assignable to $n \rightarrow \pi^*$ transition of the heteroatoms. As a result of the complexation process to the metal ion centres, these bands were shifted to 233–244 nm for $\pi \rightarrow \pi^*$ transition, while $n \rightarrow \pi^*$ transition appeared at 302–307 nm.[27] The UV–visible spectra displayed bands at 469, 467, 466, 468, 471 and 465 nm which can be attributed to charge transfer in Cr(III), Mn(II), Fe(III), Co(II), Ni(II) and Cu(II) complexes, respectively.

The diffuse reflectance spectrum of the Cr(III) complex showed three bands at 24 639, 20 465 and 14 813 cm^{-1} which may be attributed to the $^4A_{2g}(F) \rightarrow {}^4T_{2g}(F)$, $^4A_{2g}(F) \rightarrow {}^4T_{1g}(F)$ and $^4A_{2g}(F) \rightarrow {}^4T_{2g}(P)$ spin-allowed d–d transitions, respectively. The magnetic moment value was found to be 3.90 BM, which indicated the Cr(III) complex to be of octahedral geometry.[28] The Mn(II) complex exhibited four intense absorption bands at 14 763, 20 355, 24 614 and 30 230 cm^{-1}, which may be assigned to the transitions $^6A_{1g} \rightarrow {}^4T_{1g}(4G)$, $^6A_{1g} \rightarrow {}^4E_g$, $^6A_{1g} \rightarrow {}^4E_g(4D)$ and $^6A_{1g} \rightarrow {}^4T_{1g}(4P)$, respectively.[5] The magnetic moment value was found to be 5.31 BM, which indicated the Mn(II) complex to be of octahedral structure.[29] From the diffuse reflectance spectrum of the Fe(III) complex, it was observed that it exhibited a band at 35 462 cm^{-1}, which may be assigned to the $^6A_{1g} \rightarrow {}^6T_{2g}(G)$ transition in octahedral geometry. The $^6A_{1g} \rightarrow {}^5T_{1g}$ transition appeared to be split into two bands at 26 672 and 22 805 cm^{-1}. The spectrum also showed a band at 47 850 cm^{-1}, which may be assigned to ligand-to-metal charge transfer. The observed magnetic moment of the Fe(III) complex was 5.64 BM. The diffuse reflectance spectrum of the Co(II) complex showed three bands at 16 436, 17 382 and 21 102 cm^{-1} attributed to the $^4T_{1g}(F) \rightarrow {}^4T_{2g}(F)$, $^4T_{1g}(F) \rightarrow {}^4A_{2g}(F)$ and $^4T_{1g}(F) \rightarrow {}^4T_{1g}(P)$ transitions, respectively, demonstrating octahedral geometry around the Co(II) ion. [30] The observed magnetic moment of the complex was 4.61 BM. The diffuse reflectance spectrum of the Ni(II) complex showed d–d bands at 16 736, 18 215 and 25 801 cm^{-1}, which may be assigned to $^3A_{2g}(F) \rightarrow {}^3T_{2g}(F)$, $^3A_{2g}(F) \rightarrow {}^3T_{1g}(F)$ and $^3A_{2g}(F) \rightarrow {}^3T_{2g}(F)$ transitions, respectively. This proved the Ni(II) complex to be of octahedral geometry.[30] The Ni(II) complex exhibited a magnetic moment of 3.25 BM, which was representative of two unpaired electrons per Ni(II) ion and this is a further indication for the suggested octahedral geometry.[31] The diffuse reflectance spectrum of the Cu(II) complex showed d–d transition bands at 16 413, 19 586 and 26 805 cm^{-1}. These bands correspond to $^2B_{1g} \rightarrow {}^2A_{1g}(d_{x^2-y^2} \rightarrow d_{z^2})$, $^2B_{1g} \rightarrow {}^2B_{2g}(d_{x^2-y^2} \rightarrow d_{xy})$ and $^2B_{1g} \rightarrow {}^2E_g(d_{x^2-y^2} \rightarrow d_{xz}, d_{yz})$ transitions, respectively. On the basis of electronic transitions, a distorted octahedral geometry is suggested for the Cu(II) complex. The obtained magnetic moment value of 1.93 BM for the Cu(II) complex was indicative of one unpaired electron per Cu(II) ion for d^9 system suggesting spin-free distorted octahedral geometry. Both Zn(II) and Cd(II) complexes were diamagnetic and an octahedral geometry was proposed for these complexes according to the empirical formulae.

3.2.7 | Thermal analysis (TG and DTG)

The TG and DTG analyses for Schiff base ligand HL and its metal complexes were conducted within the temperature range from 50 to 1000 °C. The results are presented in Table 1.

The TG data for HL showed four stages of decomposition. The first two stages within the range 50–300 °C with temperature maxima of 90 and 225 °C correspond to loss of the $C_8H_{10}NO$ molecule with mass loss of 26.01% (calcd 26.30%). The third decomposition step was found within

TABLE 1 Thermoanalytical results (TG and DTG) for HL and its metal complexes

Complex	TG range (°C)	DTG_{max} (°C)	n^a	Mass loss (%): est. (calcd)	Total mass loss (%): est. (calcd)	Assignment	Metallic residue
HL	50–300	90, 225	2	26.01 (26.30)	99.50 (99.90)	Loss of $C_8H_{10}NO$	—
	300–605	450	1	43.24 (43.71)		Loss of $C_5H_6Br_2$	
	605–1000	730	1	30.26 (30.04)		Loss of $C_{10}H_7N_2$	
$[Cr(HL)(H_2O)Cl_2]Cl{\cdot}4H_2O$	50–165	105	1	10.05 (9.24)	84.62 (84.22)	Loss of $4H_2O$	$½Cr_2O_3$ + 4C
	165–600	310, 445	2	52.42 (51.93)		Loss of H_2O and $C_{13}H_{18}Cl_3BrN_2$	
	600–1000	690	1	22.17 (23.12)		Loss of $C_6H_7BrNO_{0.5}$	
$[Mn(HL)(H_2O)_2Cl]Cl{\cdot}3H_2O$	50–160	105	1	7.23 (7.41)	87.63 (87.01)	Loss of $3H_2O$	MnO + 2C
	160–340	265	1	38.25 (37.84)		Loss of $2H_2O$ and $C_5H_{12}Cl_2BrN$	
	340–525	395	1	34.73 (34.82)		Loss of $C_{13}H_5BrN$	
	525–1000	645	1	7.21 (7.60)		Loss of C_3H_6N	
$[Fe(HL)Cl_3]{\cdot}5.5H_2O$	50–170	110	1	10.04 (10.40)	83.66 (83.56)	Loss of $4.5H_2O$	$½Fe_2O_3$ + 4C
	170–410	275	1	43.28 (43.01)		Loss of $C_5H_8Cl_3Br_2$	
	410–605	470	1	8.17 (8.86)		Loss of C_4H_7N	
	605–1000	655	1	22.06 (22.86)		Loss of $C_{11}H_{10}N_2O_{0.5}$	
$[Co(HL)(H_2O)_2Cl]Cl$	50–390	245	1	44.18 (44.21)	84.73 (85.51)	Loss of $2H_2O$ and $C_8H_5Cl_2BrN$	CoO + 2C
	390–685	500	1	6.19 (6.72)		Loss of C_2H_8N	
	685–1000	885	1	34.37 (34.68)		Loss of $C_{11}H_{10}BrN$	
$[Ni(HL)(H_2O)_2Cl]Cl$	50–350	215	1	32.13 (31.92)	87.28 (87.30)	Loss of $2H_2O$ and $C_2H_7Cl_2Br$	NiO + C
	350–635	440	1	11.49 (11.71)		Loss of C_5H_6N	
	635–1000	795, 835	2	43.60 (43.64)		Loss of $C_{15}H_{10}BrN_2$	
$[Cu(HL)(H_2O)_3]Cl_2$	50–400	225	1	65.04 (64.82)	87.63 (87.02)	Loss of $3H_2O$ and $C_{11}H_{12}Cl_2Br_2N_2$	CuO + C
	400–1000	525	1	22.58 (22.52)		Loss of $C_{11}H_{13}N$	
$[Zn(HL)(H_2O)_2Cl]Cl{\cdot}2H_2O$	50–210	95	1	10.57 (10.00)	85.21 (85.46)	Loss of $2H_2O$ and HCl	ZnO + 2C
	210–1000	320, 635	2	74.60 (75.46)		Loss of $C_{21}H_{27}ClBr_2N_3O_2$	
$[Cd(HL)(H_2O)Cl_2]{\cdot}2H_2O$	50–150	95	1	4.10 (4.77)	87.76 (87.52)	Loss of $2H_2O$	CdO
	150–380	305	1	19.92 (19.36)		Loss of H_2O and $C_3H_7Cl_2N$	
	380–560	465	1	34.48 (35.01)		Loss of $C_8H_8Br_2$	
	560–940	630, 670	2	29.08 (28.38)		Loss of $C_{12}H_{10}N_2O$	

[a]Number of decomposition steps.

the range 300–605 °C with a temperature maximum of 450 °C, which corresponds to the loss of $C_5H_6Br_2$ molecule with mass loss of 43.24% (calcd 43.71%). The final decomposition stage in the range 605–1000 °C corresponds to complete decomposition of the remaining part of the ligand ($C_{10}H_7N_2$) with mass loss of 30.26% (calcd 30.04%). The DTG curve gave maximum peak temperature at 730 °C and the total weight loss amounted to 99.50% (calcd 99.90%).

The TG curve for the Cr(III) complex showed four weight loss stages. All of the complex decomposition occurred within the range 50–1000 °C, with four maxima at 105, 310, 445 and 690 °C. The first weight loss was typical for the loss of four molecules of water with estimated mass loss of 10.05% (calcd 9.24%). The second and third weight loss steps were related to the loss of another water molecule along with $C_{13}H_{18}Cl_3BrN_2$ fragment with estimated mass loss of 52.42% (calcd 51.93%). The final step showed a mass loss of 22.17% (calcd 23.12%) which was in accordance with the estimated loss of $C_6H_7BrNO_{0.5}$. Finally metal oxide $½Cr_2O_3$ contaminated with four carbon atoms remained as a residue. The overall weight loss amounted to 84.62% (calcd 84.22%).

The Mn(II) complex gave a decomposition pattern of four stages. The first stage occurred in the range 50–160 °C with a maximum at 105 °C and was related to the loss of three water molecules with an estimated weight loss of 7.23% (calcd 7.41%). The second decomposition step

was within the range 160–340 °C with a maximum at 265 °C, which corresponds to the loss of $C_5H_{12}Cl_2BrN$ fragment along with two water molecules with mass loss of 38.25% (calcd 37.84%). The third decomposition step was observed within the range 340–525 °C with a maximum at 395 °C, which corresponds to the loss of $C_{13}H_5BrN$ molecule with mass loss of 34.73% (calcd 34.82%). The last decomposition step occurred in the range 525–1000 °C with a maximum at 645 °C, corresponding to complete decomposition of the remaining part of the ligand (C_3H_6N) with mass loss of 7.21% (calcd 7.60%). A residue of MnO was contaminated with two carbon atoms was left from the decomposition process.

The Fe(III) complex also gave a decomposition pattern of four stages. The first stage occurred in the range 50–170 °C with a maximum at 110 °C and was related to the loss of four-and-a-half water molecules with an estimated weight loss of 10.04% (calcd 10.40%). The second decomposition step was within the range 170–410 °C with a maximum at 275 °C, which corresponds to the loss of $C_5H_8Cl_3Br_2$ fragment with mass loss of 43.28% (calcd 43.01%). The third decomposition step was observed within the range 410–605 °C with a maximum at 470 °C, which corresponds to the loss of C_4H_7N molecule with mass loss of 8.17% (calcd 8.86%). The last decomposition step occurred in the range 605–1000 °C with a maximum at 655 °C, corresponding to complete decomposition of the remaining part of the ligand ($C_{11}H_{10}N_2O_{0.5}$) with mass loss of 22.06% (calcd 22.86%). Finally a residue of metal oxide $½Fe_2O_3$ contaminated with four carbon atoms remained. The overall weight loss amounted to 83.66% (calcd 83.56%).

The Co(II) complex was thermally decomposed in three steps within the range from 50 to 1000 °C. The first decomposition step gave an estimated mass loss of 44.18% (calcd 44.21%) which occurred within the range from 50 to 390 °C with a maximum at 245 °C. This step might be attributed to the loss of two molecules of water along with a $C_8H_5Cl_2BrN$ fragment. The next decomposition step occurred over the range 390–685 °C with a maximum at 500 °C, in which the complex lost the organic fragment C_2H_8N with estimated mass loss of 6.19% (calcd 6.72%). The third decomposition stage occurred over the range 685–1000 °C with a maximum at 885 °C and was attributed to the loss of a $C_{11}H_{10}BrN$ fragment with estimated mass loss of 34.37% (calcd 34.68%). At the end of the analysis, the metal oxide (CoO) contaminated with two carbon atoms was the final product with a total estimated mass loss of 84.73% (calcd 85.51%).

The TG curve for the Ni(II) complex showed a weight loss pattern over four stages. The first step of decomposition was observed within the range 50–350 °C, with a maximum at 215 °C that corresponds to the loss of two water molecules along with $C_2H_7Cl_2Br$ fragment with estimated mass loss of 32.13% (calcd 31.92%). The second step of decomposition was observed within the range 350–635 °C, with a maximum at 440 °C, attributed to the loss of a C_5H_6N fragment, having an estimated mass loss of 11.49% (calcd 11.71%). The third and fourth steps of decomposition occurred in the range 635–1000 °C with two maxima at 795 and 835 °C and corresponded to the loss of $C_{15}H_{10}BrN_2$ fragment with estimated mass loss of 43.60% (calcd 43.64%) leaving NiO contaminated with one carbon atom as a residue. The overall weight loss was 87.28% (calcd 87.30%).

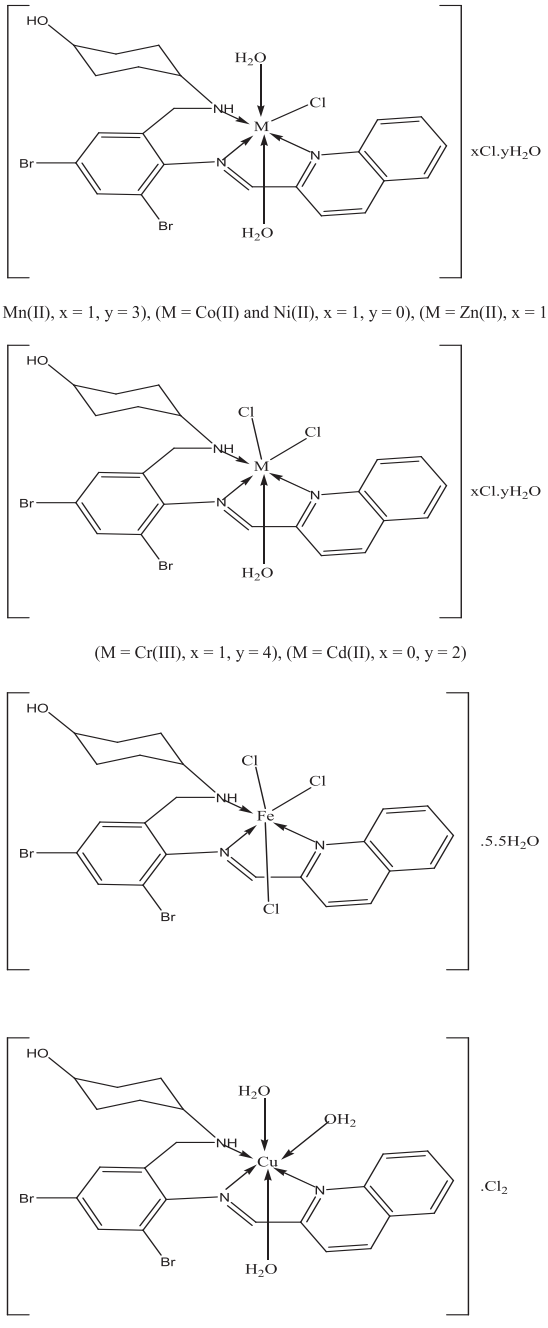

FIGURE 1 General structures of the metal complexes

The TG curve for the Cu(II) complex showed two weight loss stages. The first step of decomposition was observed within the range 50–400 °C, with a maximum at 225 °C that corresponds to the loss of three water molecules along with an organic fragment of $C_{11}H_{12}Cl_2Br_2N_2$ amounting to an estimated mass loss of 65.04% (calcd 64.82%). The second step of decomposition occurred in the range 400–1000 °C with a maximum at 525 °C corresponding to the loss of $C_{11}H_{13}N$ fragment with estimated mass loss of 22.58% (calcd 22.52%). Finally a residue of CuO contaminated with one carbon atom remained. The overall weight loss amounted to 87.63% (calcd 87.02%).

The thermogram of the Zn(II) complex showed a peak at 95 °C in the range 50–210 °C corresponding to a weight loss of 10.57% (calcd 10.00%). This step may be assigned to the loss of two water molecules as well as one mole of hydrogen chloride molecules. The next peaks were observed at 320 and 635 °C in the range 210–1000 °C and may correspond to the loss of a $C_{21}H_{27}ClBr_2N_3O_2$ fragment with estimated weight loss of 74.60% (calcd 75.46%). At the end of the thermal decomposition, the metal oxide ZnO was contaminated with two carbon atoms and remained as a residue, the total weight loss amounting to 85.21% (calcd 85.46%).

The TG curve for the Cd(II) complex exhibited five weight loss steps in the range 50–940 °C. The first step of decomposition occurred within the range 50–150 °C, with a maximum at 95 °C which corresponds to the loss of two water molecules of hydration, with estimated mass loss of 4.10% (calcd 4.77%). The next step of decomposition was observed within the range 150–380 °C, with a maximum at 305 °C that may be related to the loss of one molecule of coordinated water along with $C_3H_7Cl_2N$ fragment, where the mass loss was found to be 19.92% (calcd 19.36%). The third stage of decomposition was observed within the range 380–560 °C, with a maximum at 465 °C corresponding to the loss of a $C_8H_8Br_2$ molecule with an estimated mass loss of 34.48% (calcd 35.01%). The remaining fragment decomposed in the range 560–940 °C with a two maxima at 630 and 670 °C that may be related to the loss of a $C_{12}H_{10}N_2O$ fragment, with an estimated mass loss of 29.08% (calcd 28.38%) leaving CdO as a residue. The overall weight loss was evaluated as 87.76% (calcd 87.52%).

3.3 | Structural Interpretation

The structures of the synthesized metal complexes of HL with Cr(III), Mn(II), Fe(III), Co(II), Ni(II), Cu(II), Zn(II) and Cd(II) metal ions were characterized using elemental analysis, molar conductance, magnetic and thermal analysis data. From FT-IR spectra, it could be concluded that HL behaved as a neutral tridentate ligand coordinated to the metal ions via three nitrogen atoms. From the molar conductance data, it was found that all the complexes have an electrolyte nature except the Fe(III) and Cd(II) complexes, and the general form of the structures of the complexes is shown in Figure 1.

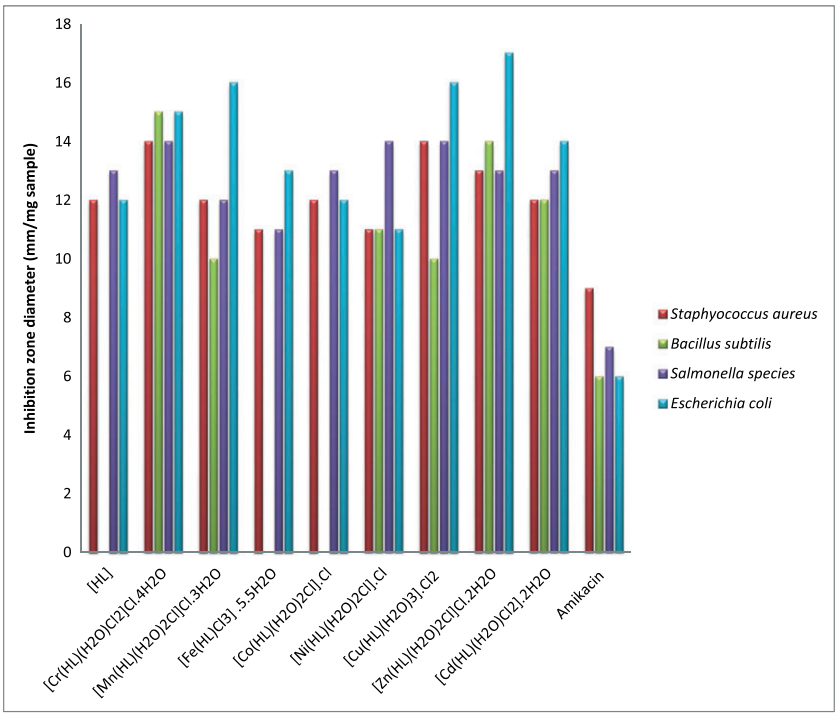

FIGURE 2 Antibacterial activity of HL and its metal complexes

3.4 | Biological Activity

It is well known that metal complexes have higher antibacterial activity than their associated free Schiff base ligand which can be attributed to the chelation of the Schiff base with metal ions[32] as metal chelates displaying both polar and non-polar properties. This makes them suitable for penetration into cells and tissues. The polarity of the metal ion will be decreased to a greater extent because of the overlap of the ligand orbital upon complexation, and partial sharing of the positive charge of the metal ion with donor groups.[33,34] Chelation enhances the delocalization of π-electrons over the whole chelating ring and induces the penetration of complexes into lipid membranes. It also increases the lipophilic and hydrophilic nature of the central metal

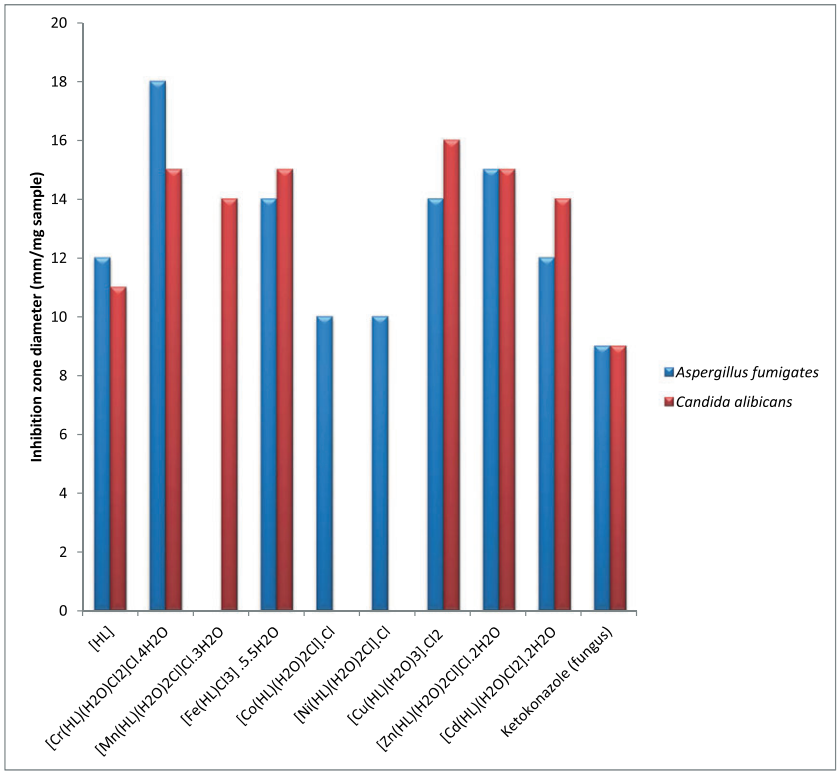

FIGURE 3 Antifungal activity of HL and its metal complexes

TABLE 2 Biological activity of HL and its metal complexes

		Inhibition zone diameter (mm/mg sample)					
		Gram-positive bacteria		Gram-negative bacteria		Fungi	
Sample		*S. aureus*	*B. subtilis*	*Salmonella* species	*E. coli*	*A. fumigates*	*C. alibicans*
HL		12	NA	13	12	12	11
$[Cr(HL)(H_2O)Cl_2]Cl{\cdot}4H_2O$		14	15	14	15	18	15
$[Mn(HL)(H_2O)_2Cl]Cl{\cdot}3H_2O$		12	10	12	16	NA	14
$[Fe(HL)Cl_3]{\cdot}5.5H_2O$		11	NA	11	13	14	15
$[Co(HL)(H_2O)_2Cl]Cl$		12	NA	13	12	10	NA
$[Ni(HL)(H_2O)_2Cl]Cl$		11	11	14	11	10	NA
$[Cu(HL)(H_2O)_3]Cl_2$		14	10	14	16	14	16
$[Zn(HL)(H_2O)_2Cl]Cl{\cdot}2H_2O$		13	14	13	17	15	15
$[Cd(HL)(H_2O)Cl_2]{\cdot}2H_2O$		12	12	13	14	12	14
Standard	Amikacin	9	6	7	6	—	—
	Ketokonazole	—	—	—	—	9	9

ions contributing to liposolubility and permeability through the lipid layer of cell membranes. Furthermore, lipophilicity, which is responsible for the rate of entry of molecules into cells, is improved by coordination, so a metal complex can become more active than the free Schiff base ligand.[5]

For HL and its metal complexes investigated in this paper, antibacterial and antifungal activities *in vitro* were determined using two Gram-negative bacteria (*Salmonella* species and *E. coli*), two Gram-positive bacteria (*B. subtilis* and *S. aureus*) and two fungi (*A. fumigatus* and *C. albicans*).

Results for the measurement of zone of inhibition against the growth of bacteria and fungi for HL and its metal complexes are shown in Figures 2 and 3 and the data summarized in Table 2. DMSO was used as a negative control and amikacin and ketokonazole were used as positive standards for antibacterial and antifungal studies.[25]

The antibacterial studies showed that, using *S. aureus* as Gram-positive bacterium, all the metal complexes have a biological activity higher than that of the free ligand, with the Cr(III) and Cu(II) complexes having the highest biological activity in comparison with the other complexes. Using *B. subtilis* as Gram-positive bacterium, the free ligand does not have any biological activity towards it. On the other hand, all the complexes showed biological activity except the Fe(III) and Co(II)complexes. The biological activity of the Cr(III) complex was the highest. Using *Salmonella* species as Gram-negative bacterium, the biological activities of Cr(III), Ni(II) and Cu(II) complexes were higher than that of the free ligand.

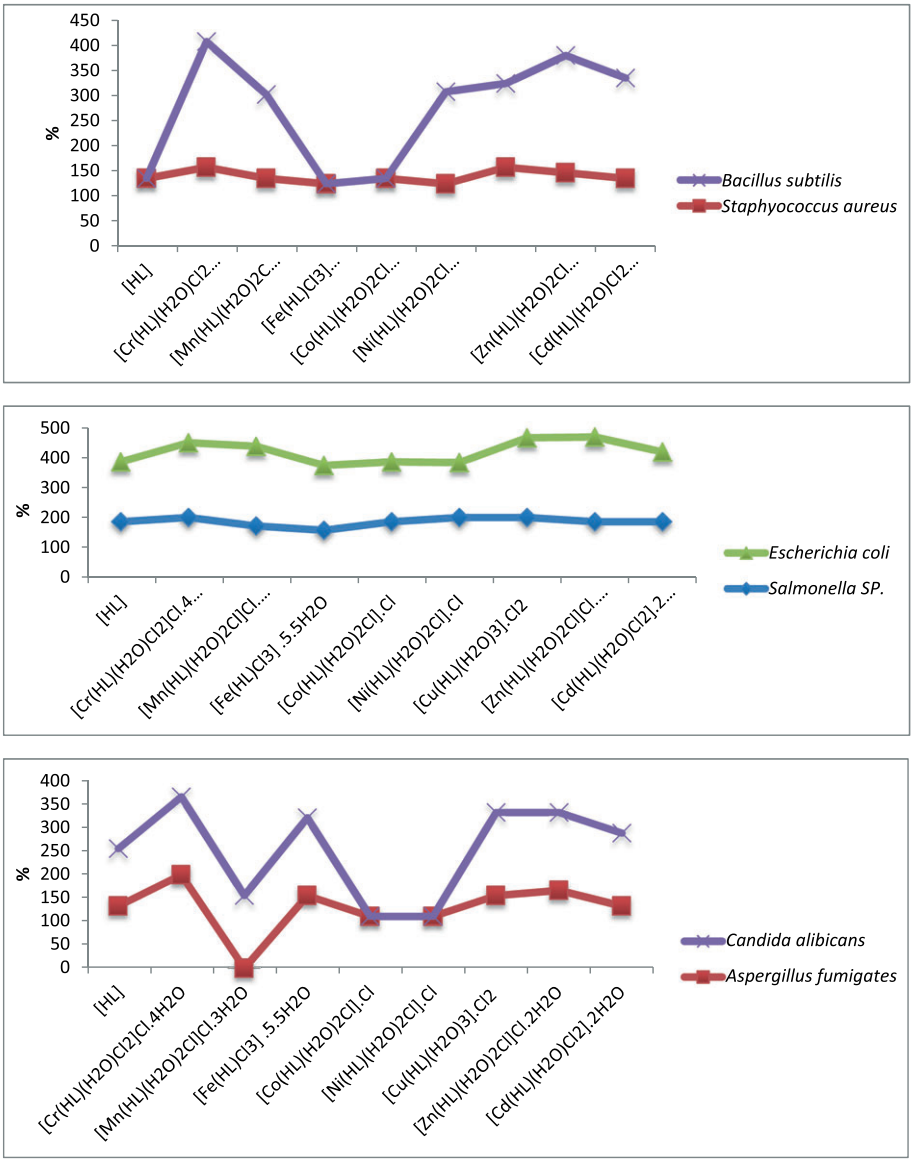

FIGURE 4 Activity index of HL and its metal complexes

In the case of Co(II), Zn(II) and Cd(II) complexes, their biological activities were the same as that of the free ligand. The activities of the other complexes were lower than that of the free ligand. Using *E. coli* as Gram-negative bacterium, the Zn(II) complex has the highest biological activity while the Ni(II) complex has the lowest.

The antifungal studies showed, using *C. albicans*, that the highest activity was that of the Cr(III) complex. On the other hand, the Mn(II) complex did not show any biological activity towards *C. albicans*. Using *A. fumigatus*, the highest activity was shown by the Cu(II) complex and the lowest activity by the free ligand. There was no biological activity for the Co(II) and Ni(II) complexes.

The activities of the prepared Schiff base ligand and its metal complexes were confirmed by calculating the activity index according to the following relationship:[32,35]

$$\text{Activity index } (A) = \frac{\text{Inhibition zone of compound (mm)}}{\text{Inhibition zone of standard drug (mm)}} \times 100$$

From the previous data, it was concluded that generally the Cr(III) complex had the highest activity index for all the investigated bacteria and fungi (Figure 4).

3.5 | Docking Study

Molecular docking studies aid the description of inhibitory potential and also can be used to predict the binding mode or mechanism of chemical moieties in the pockets of enzymes. This method is considered as a very helpful key tool in computer drug design.[36] Tumorigenesis is a complex process, and understanding the mechanisms behind it is key to identifying effective targeted therapies.[37] Due to the importance of docking studies nowadays, we were interested in docking HL and its Zn(II) complex with the receptor of breast cancer mutant oxidoreductase (PDB ID: 3HB5). Three-dimensional plots of docking are shown in Figure 5. Also, the binding energies of these compounds were calculated using computational docking studies.[38] These energy values are listed in Table 3. From these data, it is evident that the interaction between the Zn(II) complex and the 3HB5 receptor is stronger than that of its parent Schiff base depending on the low binding energy which was calculated and shown in Figure 5. Also, the binding energy decreases upon coordination. So, the complexes are more active with lower binding energy than the ligand which means that the formation of the Schiff base ligand complexes enhances the activity.

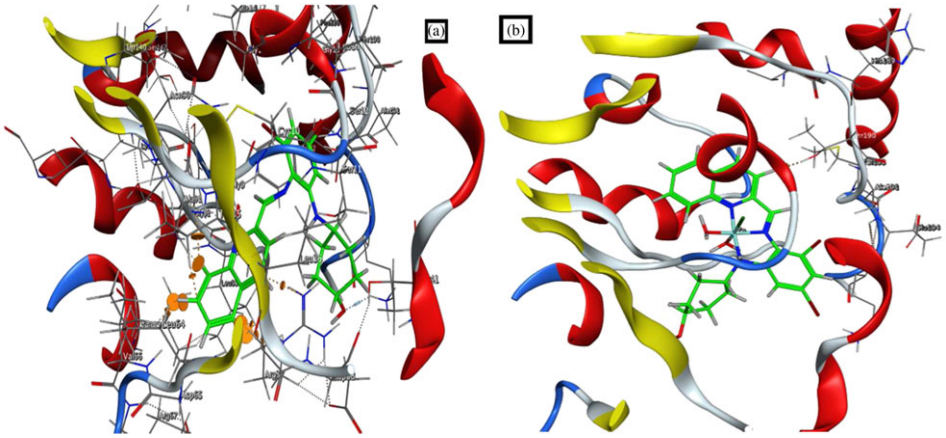

FIGURE 5 Three-dimensional plot of interaction between (a) HL and (b) $[Zn(HL)(H_2O)_2Cl]Cl{\cdot}2H_2O$ and receptor 3HB5

TABLE 3 Energy values obtained in docking calculations of HL and $[Zn(HL)(H_2O)_2Cl]Cl{\cdot}2H_2O$ with crystal structure of breast cancer (PDB ID: 3HB5)

Compound	Ligand moiety	Receptor	Interaction	Distance	E (kcal mol^{-1})
HL	BR10 10	N PHE 192	H-acceptor	3.14	−0.9
	O26 27	NZ LYS 195	H-acceptor	2.96	−2.8
	N43 44	N GLY 92	H-acceptor	3.07	−3
$[Zn(HL)(H_2O)_2Cl]Cl{\cdot}2H_2O$	Cl50 51	O SER 12	H-donor	3.03	−1.3
	O51 52	O GLY 92	H-donor	2.57	−6.5
	O26 27	NE ARG 37	H-acceptor	3.26	−1.2
	6-ring	6-ring PHE 192	π–π	3.88	0

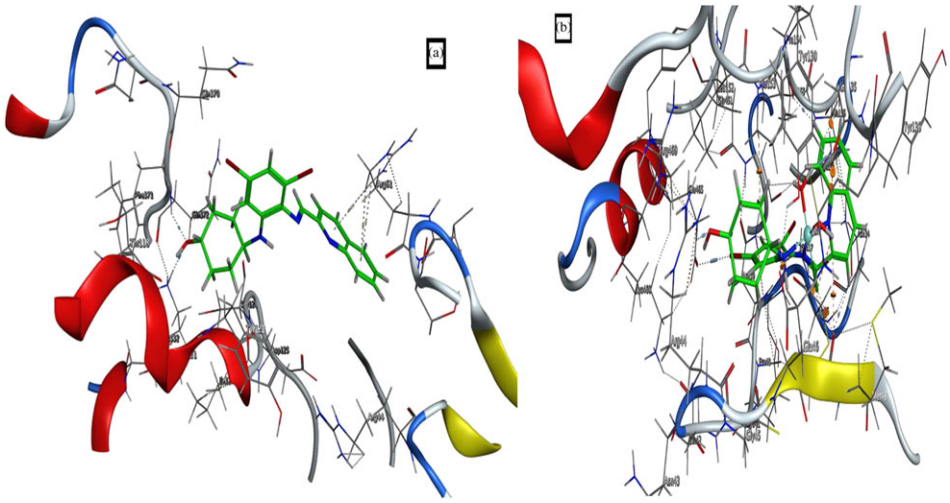

FIGURE 6 Three-dimensional plot of interaction between (a) HL and (b) $[Zn(HL)(H_2O)_2Cl]Cl{\cdot}2H_2O$ and receptor 1CX

TABLE 4 Energy values obtained in docking calculations of HL and $[Zn(HL)(H_2O)_2Cl]Cl{\cdot}2H_2O$ with crystal structure of COX-2 oxidoreductase (PDB ID: 1CX)

Compound	Ligand moiety	Receptor	Interaction	Distance	E (kcal mol^{-1})
HL	O26 27	N GLN 372	H-acceptor	3.23	−1
	O26 27	NZ LYS 532	H-acceptor	3.35	−1.2
	6-ring	CD ARG 61	π–H	4.12	−0.6
	6-ring	CD ARG 61	π–H	4.46	−0.6
	6-ring	NH1 ARG 61	π–cation	4.52	−1.5
	6-ring	NH1 ARG 61	π–cation	4.38	−0.7
$[Zn(HL)(H_2O)_2Cl]Cl{\cdot}2H_2O$	BR10 10	OE1 GLU 465	H-donor	3.3	−5.5
	C23 24	SG CYS 36	H-donor	3.77	−1
	C32 33	SG CYS 36	H-donor	3.95	−1
	C39 40	O PRO 154	H-donor	3.16	−0.9
	O51 52	O GLY 135	H-donor	2.7	−17
	O26 27	NH1 ARG 44	H-acceptor	2.53	−0.3

Prostaglandins are involved in normal physiological functions and they are involved with tumour cell growth while overexpressing.[39] Inhibition of prostaglandin synthesis is the primary target of several nonsteroidal anti-inflammatory drugs, and cyclooxygenase (COX) is an essential enzyme in prostaglandin formation. COX-2 is an inducible form of the enzyme that is usually not expressed in normal tissue.[39] COX-2 receptor overexpression increases in the production of mutagens, which further causes DNA damage as tumour initiators (prostaglandin formation). Docking studies were performed for HL and its Zn(II) complex to identify the mode of binding and binding affinity with the COX-2 receptor (PDB ID: 1CX2) (Figure 6). This study reveals that both compounds bind in the active site of COX-2 (Table 4). The Zn(II) complex showed low binding energy (−17 kcal mol^{-1}) with the selective amino acid (O GLY 135) by H-bond interaction of the COX-2. It is universally accepted that the lower the relative binding free energy, the more potent is the binding affinity between DNA and target molecules.

4 | SUMMARY AND CONCLUSIONS

New Cr(III), Mn(II), Fe(III), Cu(II), Ni(II), Co(II), Zn(II) and Cd(II) complexes with Schiff base ligand HL were prepared and characterized. HL acted as a neutral tridentate ligand through three nitrogen atoms and all the complexes showed octahedral geometry. All complexes were electrolytes except Fe(III) and Cd(II) complexes. From elemental analysis data, the complexes had composition of the MHL type with general formulae $[M(HL)(H_2O)_xCl_y]Cl_n{\cdot}(H_2O)_m$ which were differentiated

according to the metal ion. The biological activities of some of the complexes were higher than that of the free ligand. The Cr(III) complex had the highest activity index.

ORCID

Walaa H. Mahmoud http://orcid.org/0000-0001-9187-4325
Gehad G. Mohamed http://orcid.org/0000-0002-1525-5271

REFERENCES

[1] D. N. Dhar, P. N. Saxena, S. Kumar, *J. Sci. Ind. Res.* **2009**, *68*, 181.

[2] P. Rajesh, S. Gunasekaran, A. Manikandan, *J. Mol. Struct.* **2017**, *1144*, 379.

[3] H. Shargh, M. A. Nasseri, *Bull. Chem. Soc. Japn* **2003**, *76*, 137.

[4] S. K. Tobriya, *Int. J. Sci. Res.* **2014**, *3*, 1254.

[5] R. G. Deghadi, G. G. Mohamed, W. H. Mahmoud, *Appl. Organomet. Chem.* **2016**, *30*, 221.

[6] M. R. H. Keypour, *Coord. Chem. Rev.* **2014**, *280*, 203.

[7] M. Malerba, B. Ragnoli, *Expert Opin. Drug Metab. Toxicol.* **2008**, *4*, 1119.

[8] T. Weiser, *Neurosci. Lett.* **2006**, *395*, 179.

[9] C. de Mey, H. Peil, S. Kölsch, J. Bubeck, J. M. Vix, *Arzneimittelforschung* **2008**, *58*, 557.

[10] A. McNeill, J. Magalhaes, C. Shen, K. Y. Chau, D. Hughes, A. Mehta, T. Foltynie, J. M. Cooper, A. Y. Abramov, M. Gegg, A. H. Schapira, *Brain* **2014**, *137*, 1481.

[11] M. A. Burmeister, L. Bartlett, M. S. Rinaldi, M. G. Pfaller, *J. Clin. Microbiol.* **1988**, *26*, 1437.

[12] Reference method for broth dilution antifungal susceptibility testing of conidium-forming filamentous fungi: proposed standard M38-A, National Committee for Clinical Laboratory Standards, Wayne, PA, **2002**.

[13] Method for antifungal disc diffusion susceptibility testing of yeast: proposed guideline M44-P, National Committee for Clinical Laboratory Standards, Wayne, PA, **2003**.

[14] G. G. Mohamed, M. M. I. El-Dessouky, W. H. Mahmoud, *Spectrochim. Acta A* **2014**, *122*, 598.

[15] I. Sakıyan, E. Logoglu, S. Arslan, N. Sari, N. Şakiyan, *Biometals* **2004**, *17*, 115.

[16] M. Yan, Y. Li, Z. Wu, C. Yan, K. Zheng, *J. Med. Chem.* **2016**, *109*, 47.

[17] N. F. Mahmoud, G. G. Mohamed, W. H. Mahmoud, *J. Organomet. Chem.* **2017**, *848*, 288.

[18] S. A. Zaitone, A. M. Ammar, S. A. Sallam, M. A. Mahmoud, *J. Mol. Struct.* **2016**, *18*, 60.

[19] S. Devi, D. Kumar, G. Kumar, *J. Mol. Struct.* **2016**, *1108*, 680.

[20] R. Xing, S. Liu, H. Yu, P. Wang, C. Li, P. Li, Z. Guo, *Bioorg. Med. Chem. Lett.* **2005**, *15*, 4600.

[21] K. Poonia, S. Siddiqui, M. Arshad, D. K. Neelima, *Spectrochim. Acta A* **2016**, *155*, 146.

[22] G. A. Kolawole, P. O. Brien, M. Helliwell, J. Raftery, P. A. Ajibade, *Inorg. Chim. Acta* **2006**, *359*, 3111.

[23] N. Mahalakshmi, R. Rajavel, *Arabian J. Chem.* **2014**, *7*, 509.

[24] M. A. Diab, A. A. El-Bindary, M. I. Abou-Dobara, H. A. Seyam, A. Z. El-Sonbati, *J. Mol. Liq.* **2016**, *218*, 434.

[25] C. M. Sharaby, *Spectrochim. Acta A* **2007**, *66*, 1271.

[26] E. H. Ismail, G. G. Mohamed, M. M. H. Khalil, A. B. Kamel, E. M. Zayed, *Monatsh. Chem.* **2014**, *145*, 755.

[27] S. Raj, N. Naik, K. H. K. Naik, *Spectrochim. Acta A* **2014**, *15*, 599.

[28] A. B. P. Lever, *Inorganic Electronic Spectroscopy*, 2nd ed., Elsevier, New York **1997**.

[29] F. A. Cotton, G. Wilkinson, C. A. Murillo, M. Bochmann, *Advanced Inorganic Chemistry*, 6th ed., Wiley, New York **1999**.

[30] S. Chandra, B. S. Saraswat, D. Yadav, P. Tyagi, *Spectrochim. Acta A* **2015**, *15*, 155.

[31] S. Chandra, Ruchi, K. Qanungo, S. K. Sharma, *Spectrochim. Acta A* **2011**, *79*, 1326.

[32] R. S. Joseyphus, M. S. Nair, *Mycobiology* **2008**, *36*, 93.

[33] V. L. Siji, M. R. Sudarsanakumar, S. Suma, *Transition Met. Chem.* **2011**, *36*, 417.

[34] B. Türkkan, B. Sarıboğa, N. Sarıboğa, *Transition Met. Chem.* **2011**, *36*, 679.

[35] M. Habib, A. Beyramabadi, S. Allameh, M. Khashi, A. Morsali, M. Pordel, C. Khorsandi, *J. Mol. Struct.* **2017**, *1143*, 424.

[36] A. Rauf, A. Shah, K. S. Munawar, S. Ali, M. N. Tahir, M. Javed, A. M. Khan, *Arabian J. Chem.* **2017**. https://doi.org/10.1016/j.arabjc.2017.09.015

[37] A. Heydari, S. Shahraki, *Colloids Surf. B. Biointerfaces* **2017**, *160*, 564.

[38] J. Tang, J. Liu, F. Wu, *Bioorg. Chem.* **2016**, *69*, 29.

[39] S. Thangavel, M. Paulpandi, H. B. Friedrich, K. Murugan, S. Kalva, A. A. Skelton, *J. Inorg. Biochem.* **2016**, *159*, 50.

How to cite this article: Mahmoud WH, Mohamed GG, Elsawy HA, Radwan MA. Metal complexes of novel Schiff base derived from the condensation of 2-quinoline carboxaldehyde and ambroxol drug with some transition metal ions. *Appl Organometal Chem*. 2018;e4392. https://doi.org/10.1002/aoc.4392